Journal of Catalysis 278 (2011) 102–110

Contents lists available at ScienceDirect

Journal of Catalysis

journal homepage: www.elsevier.com/locate/jcat

Catalytic behavior of 1-(2-pyridylazo)-2-naphthol transition metal complexes encapsulated in Y zeolite

I. Kuźniarska-Biernacka [a], K. Biernacki [b], A.L. Magalhães [b], A.M. Fonseca [a], I.C. Neves [a,*]

[a] Departamento de Química, Centro de Química, Universidade do Minho, Campus de Gualtar, 4170-057 Braga, Portugal
[b] REQUIMTE, Departamento de Química e Bioquímica, Faculdade de Ciências, Universidade do Porto, Rua do Campo Alegre, 4169-007 Porto, Portugal

ARTICLE INFO

Article history:
Received 18 October 2010
Revised 29 November 2010
Accepted 29 November 2010
Available online 31 December 2010

Keywords:
NaY
Heterocyclic ligand
Metal complexes
Encapsulation
Oxidation

ABSTRACT

The goal of this study is the preparation of new heterogeneous catalysts to be used in the oxidation of organic molecules under mild conditions. The metals in zeolite (M–Y) were prepared by the *ion exchange method*. The *in situ* encapsulation of selected transition metal complexes as a guest, namely cobalt(II), nickel(II), copper(II), and zinc(II), with 1-(2-pyridylazo)-2-naphthol (PAN) ligand in supercages of Y zeolite (host) was accomplished by the *flexible ligand method*. The coordination geometry of neat and Y-encapsulated metal complexes has been determined by molecular simulations. The resulting catalysts were fully characterized by different techniques (FTIR, SEM, and chemical analysis), and the results indicated that complexes were encapsulated in supercages of Y zeolite. Catalytic studies were performed in liquid phase for cyclohexene and cyclohexanol oxidations, by using *tert*-butylhydroperoxide as the oxidizing agent at 40 and 60 °C, respectively. All prepared catalysts exhibited catalytic activity for the oxidation reactions.

1. Introduction

Oxidation is an important method for the synthesis of chemical intermediates in the manufacture of high tonnage commodities, high-value fine chemicals, agrochemicals, and pharmaceuticals, but oxidation is often an inefficient process. The introduction of heterogeneous catalysts offers obvious advantages: ease of product and catalyst recovery and suitability for continuous processing. Consequently, heterogenization of homogeneous catalysts has become an important strategy for obtaining supported catalysts that retain the active catalytic sites of the homogeneous analog while providing the advantages of a heterogeneous catalyst [1,2].

Zeolite encapsulation of transition metal complexes with oxidation catalytic activity is one example of these heterogenization strategies and also is a theme of current research. Several approaches have been used for the encapsulation of transition metal complexes in zeolite supercages, the choice of any specific method being dictated by the size of the ligand relative to the free diameter of the zeolite channels. Complexes or ligands that are smaller than the channels can be adsorbed from a solution phase into the zeolite, or they can be synthesised via diffusion of the ligand by the *flexible ligand method* into a metal-exchanged zeolite [3–6]. These new host–guest materials are interesting for application as biomimetic heterogeneous catalysts for the oxidation of alkanes, alkenes, and alcohols [1–10].

The oxyfunctionalization of inexpensive hydrocarbons to produce more valuable organic compounds such as alcohols, aldehydes, and ketones requires the selective oxidation of strong C–H bonds. Alcohols and ketones are important intermediate materials for the manufacture of many important products, such as fiber, drugs, and fragrance. Maurya et al. have encapsulated oxovanadium(IV) and copper(II) complexes with amino acid as well as Schiff base ligands in the zeolite Y and studied their catalytic potentialities for the oxidation of unsaturated hydrocarbons [11,12]. Alumina-supported manganese(II) complexes with nitrogen and oxygen donor ligands catalyze, in presence of peroxides, the oxidation of cyclohexene in moderate yield [13], and also transition metal complexes with tetradentate Schiff base ligand entrapped in the cavity of Y zeolite have also been used as catalysts for this reaction [14]. It was also found that transition metal complexes selectively catalyzed the oxidation of cyclohexanol into ketone. Manganese(II) complexes both in homogeneous and in heterogeneous phases can act as selective catalysts in this reaction [15,16], as chromium immobilized on silica-based materials [17] as well as tungsten-based catalysts [18].

The objective of the present work is to evaluate the catalytic behavior of the transition metal complexes with 1-(2-pyridylazo)-2-naphthol (PAN) ligand encapsulated in Y zeolite. The guest–host catalysts, [M(PAN)]@Y where M represents metal ion (Co(II), Ni(II), Cu(II), and Zn(II)), were evaluated in oxidation of cyclohexene and

* Corresponding author.
E-mail address: ineves@quimica.uminho.pt (I.C. Neves).

0021-9517/$ - see front matter © 2010 Elsevier Inc. All rights reserved.
doi:10.1016/j.jcat.2010.11.022

cyclohexanol in liquid phase using *tert*-butylhydroperoxide (tBuOOH) as an oxygen source.

2. Experimental section

2.1. Materials and reagents

The NaY zeolite (Si/Al = 2.83) in powder form was obtained from Zeolyst International. It was calcined at 500 °C during 8 h under a dry air stream prior to use. The PAN ligand was purchased from Aldrich. For the encapsulation and the synthesis of neat complexes, solvents and chemicals were purchased from Aldrich and were used as received unless otherwise specified. Nitrate metal salts (Aldrich) [$Co(NO_3)_2{\cdot}6H_2O$, $Ni(NO_3)_2{\cdot}6H_2O$, $Cu(NO_3)_2{\cdot}3H_2O$, and $Zn(NO_3)_26H_2O$] were used for the preparation of M–Y. The neat complexes were prepared with chloride salts of respective metals ($CoCl_2{\cdot}6H_2O$, $NiCl_2{\cdot}6H_2O$, $CuCl_2{\cdot}2H_2O$, and $ZnCl_2$) from Aldrich. KBr used for the FTIR pellets preparation was from Merck, spectroscopic grade. DMF used for UV–visible spectra was from Aldrich, spectrophotometric grade. All other chemicals and solvents used for the catalytic reactions were reagent grade and purchased from Aldrich.

2.2. Synthesis of neat PAN complexes

The PAN complexes were obtained by standard methods [19,20]. Briefly, a solution of ligand in methanol was added to a solution of the respective metal chloride in the same solvent (metal:ligand molar ratio = 1:1). Elemental analysis of [M(PAN)Cl] complexes confirmed the purity of obtained compounds and shows that in all cases the complexes with mixed ligands are formed with the metal:PAN:chloride 1:1:1 M ratio. Analytical data for the neat complexes with 1:1 metal:PAN molar ratio are as follows: [Cu(PAN)Cl]; Purple solid (yield 67%). Recrystallized from CH_2Cl_2/Et_2O. λ_{max} = 564.5, 549.0, 530.5 nm. HRMS (NBA): *m*/*z* for $C_{15}H_{10}CuN_3OCl$; calcd. 345.9802; found 345.9799. Anal. Calcd. for $C_{15}H_{10}CuN_3OCl$; C 51.88, H 2.90, N 12.10. Found: C 51.76, H 3.02, N 12.21.

[Ni(PAN)Cl]; Red solid (yield 76%). Recrystallized from CH_2Cl_2/Et_2O. λ_{max} = 568.0, 529.0, 485.0 nm. HRMS (NBA): *m*/*z* for $C_{15}H_{10}NiN_3OCl$; calcd. 340.9860; found 340.9861. Anal. Calcd. for $C_{15}H_{10}NiN_3OCl$; C 52.62, H 2.94, N 12.27. Found: C 52.45, H 2.88, N 12.37.

[Co(PAN)Cl]; Green solid (yield 72%). Recrystallized from CH_2Cl_2/Et_2O. λ_{max} = 621.0, 580.0, 530.0 nm. HRMS (NBA): *m*/*z* for $C_{15}H_{10}CoN_3OCl$; calcd. 341.9838; found 341.9832. Anal. Calcd. for $C_{15}H_{10}CoN_3OCl$; C 52.62, H 2.94, N 12.27. Found: C 52.24, H 2.90, N 12.41.

[Zn(PAN)Cl]; Red (yield 70%). Recrystallized from CH_2Cl_2/Et_2O. λ_{max} = 555.0, 543.0, 528.0 nm. HRMS (NBA): *m*/*z* for $C_{15}H_{10}ZnN_3OCl$; calcd. 346.9798; found 346.9800. Anal. Calcd. for $C_{15}H_{10}ZnN_3OCl$; C 51.61, H 2.89, N 12.04. Found: C 51.88, H 2.95, N 12.21.

The [$Ni(PAN)_2$] complex was obtained using standard methods. Briefly, a solution of ligand in methanol was added to a solution of nickel(II) chloride in the same solvent (metal:ligand molar ratio = 1:2). Elemental analysis of [$Ni(PAN)_2$] complex confirms the purity of obtained compound. [$Ni(PAN)_2$]; dark brown solid (yield 73%). λ_{max} = 810.0, 569.0, 529.0, 500_{sh} nm. Anal. Calcd. for $C_{30}H_{20}NiN_6O_2$; C 64.90, H 3.63, N 15.4. Found: C 64.33, H 3.92, N 14.73.

2.3. Encapsulation of the transition metal complexes with PAN ligand in NaY zeolite

The encapsulation of [Cu(PAN)] and [Co(PAN)] guests has been described elsewhere [20,21]. The encapsulation of nickel(II) and zinc(II) PAN complexes was based on a previously established procedure [22]. Briefly, encapsulation starts with a cation exchange in NaY zeolite using aqueous solution of hydrated metal(II) nitrate (3.73×10^{-1} mmol) per 1.0 g of NaY (previously dried at 150 °C during 12 h). The resulting mixture was stirred for 12 h at room temperature, and pale pink, pale green, pale blue, and white suspensions were obtained for cobalt(II), nickel(II), copper(II), and zinc(II), respectively. The solid was filtered off and dried in an oven at 60 °C for 12 h and finally dried in vacuum for 2 h. A solution of PAN (7.55×10^{-1} mmol) in 50 mL THF was added to the metal-exchanged NaY (PAN:Metal(II) = 2:1 M ratio). The suspensions were stirred for 12 h at room temperature. The suspensions turned green, brownish red, dark red, and yellow for cobalt(II), nickel(II), copper(II), and zinc(II), respectively, within a few min. of the beginning of the reaction. The obtained guest–host catalysts were filtered off. Before characterization, the samples were Soxhlet extracted for 12 h in ethanol to remove the remaining uncomplexed ligand and the species adsorbed on the external surface of the zeolite. The guest–host catalysts obtained were denoted as [M(PAN)]@Y where M represents metal ion (Co(II), Ni(II), Cu(II), and Zn(II)).

2.4. Characterization procedures

The quantitative analysis of the elements, Si, Al, Na, and M, was carried out by inductively coupled plasma atomic emission spectrometry (ICP-AES) using a Philips ICP PU 7000 Spectrometer. Chemical analysis of C, H, and N was carried out on a Leco CHNS-932 analyzer. ^{1}H NMR spectra were obtained on a Varian Unity Plus Spectrometer at an operating frequency of 300 MHz using the solvent peak as internal reference at 25 °C. All chemical shifts are given in ppm using δ_H Me_4Si = 0 ppm as reference. High-resolution mass spectra (HRMS) were obtained with a GV AutoSpec spectrometer using an *m*-nitrobenzyl alcohol (NBA) matrix. Room temperature Fourier transform infrared (FTIR) spectra of diluted 4% in KBr pellets were measured using a Bomem MB104 spectrometer in the range 4000–500 cm^{-1} by averaging 32 scans at a maximum resolution of 4 cm^{-1}. The electronic UV–visible absorption spectra of neat complexes were collected over the wavelength the range of 600–200 nm with a Shimadzu UV/2501PC spectrophotometer using quartz cells at room temperature in DMF. Scanning electron micrographs (SEM) were performed on a FEI Nova 200 scanning electron microscope equipped with an EDS system (EDAX – Pegasus X4M (EDS/EBSD)). The GC-FID chromatograms were obtained with SRI 8610C chromatograph using nitrogen as carrier gas and CP-Sil 8CB capillary column for quantification of the products. The identities of these reaction products were confirmed by GC–MS (Varian 4000 Performance).

2.5. Computational details

The geometries of all transition metal complexes Co(II), Ni(II), Cu(II) [20], and Zn(II) with the PAN ligand, for 1:1 metal:PAN molar ratio and for Ni(II) also with 1:2 M ratio, were characterized by a quantum mechanical method based on density functional theory (DFT). The B3LYP Becke's three-parameter exchange–correlation hybrid functional with nonlocal correlation corrections, provided by Lee, Yang, and Parr, was used [23–26]. The double-zeta Pople basis set 6-31G(d,p) was employed, which ensures a superior electronic description by adding polarization functions of the *p*-type, *d*-type, and specially *f*-type for all hydrogen, non-hydrogen atoms, and metal ions, respectively. Full geometry optimization of the molecular system was performed in the gas phase without any symmetry restriction. The geometry optimization was always started with the metal ion out of plane defined by the oxygen,

the two nitrogen, and the chloride coordinating atoms, in order to avoid metastable structures.

The vibration frequencies for the neat PAN complexes were calculated employing a harmonic model considering the molecules as being isolated in the gas phase. The vibrational frequencies of these optimized structures were predicted using the same basis set. No imaginary frequencies were obtained, which confirms that the molecular structures were optimized to a stationary position on the potential energy surface. Usually, the harmonic frequencies are calculated at B3LYP/6-31G(d,p) level have to be scaled [27–29]. However, due to quite a good agreement between our theoretical and experimental results (see section below), the calculated frequencies were used without scaling.

All calculations were made with the Gaussian03 program package [30]. Graphical representations of the optimized structures and the molecular orbitals were produced with the MOLEKEL 4.3 package [31] and Gauss-View molecular visualization program [32].

2.6. Catalytic experiments

All catalysts were dehydrated, in vacuum for 2 h at 120 °C, prior to their use for the catalytic reaction. All blank experiments: without catalyst and using parent NaY zeolite as catalyst, were performed under the same conditions as the catalyzed reactions.

2.6.1. Oxidation of cyclohexene

In a typical reaction, tBuOOH (1.0 mL of 5.5 M in decane solution), cyclohexene (0.2 mL, 2.0 mmol), toluene (0.2 mL, 1.9 mmol), and the catalyst (0.05 g) were mixed in decane (2 mL), and the reaction mixture was heated at 30 °C (±5 °C) with continuous stirring in an oil bath. The progress of the reaction was monitored as a function of time by withdrawing portions of the sample at fixed time intervals and analysing them by gas chromatography. The identities of the products were confirmed by comparison with authentic samples or by GC–MS. The products were quantitatively determined by the internal standard method. The guest–host catalysts catalyzed the oxidation of cyclohexene into a variety of products such as 2-cyclohexene-1-ol (CyOL), 2-cyclohexene-1-one (CyONE), and 1-*tert*-butylperoxy-2-cyclohexene (CyOX), which are the typical expected products for this reaction [33,34]. After the catalytic run, the catalysts were washed twice with 20 mL of methanol and once with 20 mL of chloroform, dried in an oven at 120 °C over night under vacuum, and characterized.

2.6.2. Oxidation of cyclohexanol

The reaction was carried out in 4.0 mL of acetonitrile at 40 °C (±5 °C) with constant stirring, and the composition of the reaction medium was cylohexanol (0.6 mL, 5.8 mmol), chlorobenzene (0.6 mL, 5.9 mmol (internal standard)), and 0.10 g of heterogeneous catalyst. The oxidant, tBuOOH (2 mL of 5.5 M in decane solution), was progressively added to the reaction medium using a KD Scientific Syringe Pump: KDS 200P at a rate of 0.1 mL min^{-1}. The reaction products were analyzed and identified as mentioned above. After the reaction, the catalysts were washed, dried, and characterized.

3. Results and discussion

3.1. Theoretical studies

It is known that the PAN ligand reacts with different metal ions to give intensively colored chelate complexes. It acts as a tetradentate ligand coordinating with the metal through the hydroxyl oxygen atom, the pyridine nitrogen atom, and one of the azo-group nitrogen atoms. When the metal:ligand ratio is 1:1, the complexes show an exact or slightly distorted square co-planar geometry [19]. For the complexes with 1:2 metal:PAN molar ratio, the pseudo-octahedral geometry was found [35].

The optimization of the molecular structures for all neat PAN complexes [M(PAN)Cl] with divalent metal ions (M = Co, Ni, Cu and Zn) and the [$Ni(PAN)_2$] complex was performed in gas phase at the B3LYP/6-31G(d,p) level without any type of symmetry constraints, and typical results are depicted in Figs. 1 and 2.

The optimized values of the most relevant geometrical parameters for the [M(PAN)Cl] type complexes and for the [$Ni(PAN)_2$] complex are summarized in Tables 1 and 2, respectively.

All optimized structures of the [M(PAN)Cl] type complexes show a square-planar configuration chromophore, with coordination made by the chloride ion, oxygen, and two nitrogen atoms from the ligand (see Fig. 1a). However, the [Zn(PAN)Cl] complex has shown some distortion. In fact, the zinc atom and a specially the chloride ion (Fig. 1 b) have moved out of the plane, as confirmed by the dihedral angles N(27)—N(18)—O—M and O—N(18)—N(27)—Cl are 168.93° and 45.95°, respectively. Moreover, the dihedral angle C(9)—N(18)—N(19)—C(20), which includes the N=N bridge, also confirmed a distortion of the zinc(II) complex. In the case of copper(II) complex, only a very small distortion from the plane (ca. 2°) was observed for chloride ion; the dihedral angle O—N(18)—N(27)—Cl is 1.77°. The optimized values of the distances and angles between copper(II) ion and PAN donor atoms are in good agreement with values found from the X-ray-determined structure of the [$Cu(PAN)(NO_3)$] complex [19]. The distance difference is less than ~0.02 Å and less than ~0.8° for the angles. The most relevant distances to the metal ion (metal donors) for all complexes change in accordance with the radius of divalent metal ion (according to Shannon [36], the values of these radii (in Å) considering a four-coordinated metal environment are the following: Co^{2+} = 0.58, Ni^{2+} = 0.55, Cu^{2+} = 0.57, and Zn^{2+} = 0.60). An exception is the zinc(II) complex where the distance Zn—Cl is shorter than

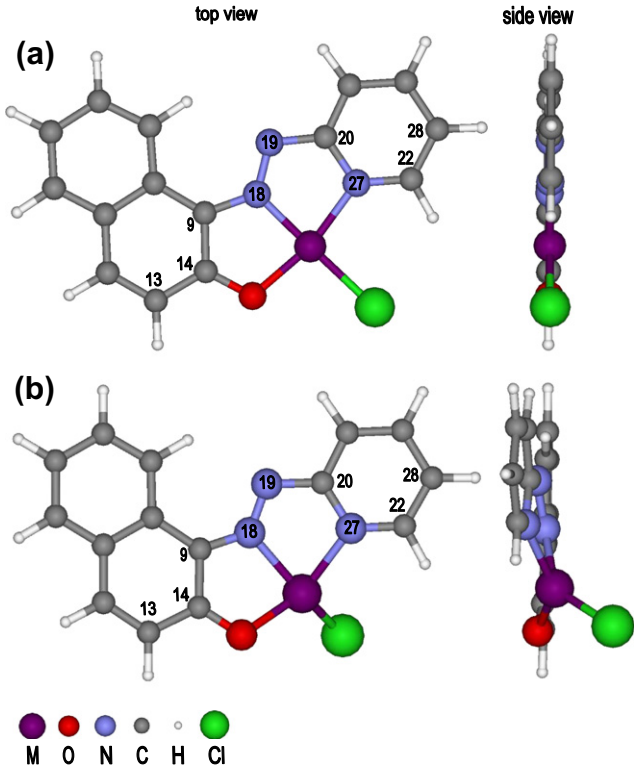

Fig. 1. Optimized structures for neat PAN complexes: (a) square-planar coordination, M = Co(II), Ni(II), and Cu(II) and (b) distorted planar coordination, M = Zn(II).

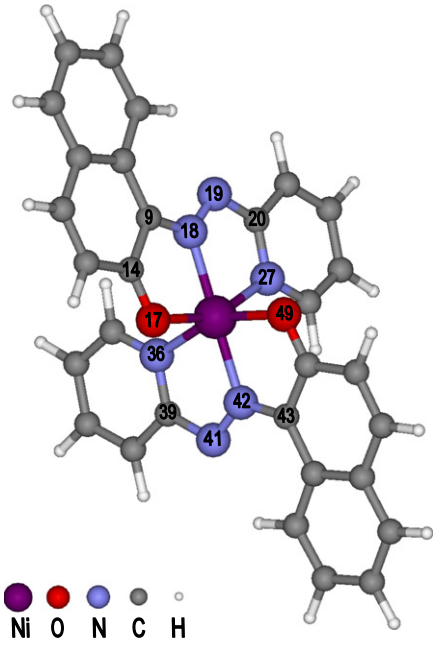

Fig. 2. The optimized structure for the six-coordinate nickel(II) complex with PAN ligand (complex obtained from 1:2 Ni:PAN molar ratio).

Table 2
Selected distances, angles, and dihedral angles for six-coordinate [Ni(PAN)$_2$] complex; calculated in vacuum at B3LYP/6-31G(d,p) level.

Complex[a]	[Ni(PAN)$_2$]	
	L	*L′*
Distance (Å)		
Ni—N(18) or (42)	2.023	2.023
Ni—N(19) or (41)	2.900	2.900
Ni—N(27) or (36)	2.095	2.096
Ni—O(17) or (49)	2.056	2.056
Angle (°)		
O(17)—Ni—N(18)	79.67	
N(18)—Ni—N(27)	77.04	
N(27)—Ni—N(42)	103.57	
N(42)—Ni—O(17)	99.72	
N(18)—Ni—N(42)	179.31	
O(17)—Ni—N(27)	156.71	
N(36)—Ni—O(49)	156.71	
Dihedral angle (°)		
O(17)—N(18)—N(27)—N(42)	0.39	
O(49)—N(18)—N(36)—N(42)	0.55	
C(20)—N(19)—N(18)—Ni	0.18	
C(39)—N(41)—N(42)—Ni	0.05	
O(17)—N(18)—N(27)—Ni	0.19	
O(49)—N(42)—N(36)—Ni	0.28	
O(17)—N(18)—N(19)—N(27)	0.98	
O(49)—N(42)—N(41)—N(36)	1.06	
C(9)—N(18)—N(19)—C(20)	179.24	
C(39)—N(41)—N(42)—C(43)	179.22	
N(18)—N(19)—C(20)—C(27)	1.02	
N(19)—N(18)—C(9)—C(14)	179.59	

[a] Atom numbering as referred in Fig. 2.

that in the case of the copper(II) complex. The shorter M—Cl distance for the zinc(II) complex when compared to copper(II) complex is due to a distortion of square-planar coordination of the metal. Of all optimized values of the distances, that of the nickel(II) complex is the smallest.

The 1:2 Ni:PAN molar ratio for the complex with nickel(II) was confirmed by elemental analysis. The optimized structure of [Ni(PAN)$_2$] complex, which was obtained during encapsulation into zeolite, shows pseudo-octahedral geometry. The optimization process, carried out without any constraints, provides a complex framework structure. The metal ion in this complex is coordinated by two perpendicularly planar azo chromophoric ligands. The coordination bond lengths, which are one of the most important points in the metal complex structure, were well reproduced (Table 2). The calculated Ni—N and Ni—O bond lengths (~2.0 Å) are consistent with the typical lengths in the octahedral coordinate Ni(II) complexes [37,38]. The corresponding bond lengths of the [Ni(PAN)$_2$] complex are longer than those of the square-planar coordinate Ni(II) complexes ([Ni(PAN)Cl] – Table 1). The typical lengths of the corresponding bonds for the square-planar coordinate Ni(II) complexes are 1.8–1.9 Å [39]. Due to the larger distances between the donor atoms and the metal ion, the corresponding angles of the donor atoms of PAN ligand and metal ion are more acute for the [Ni(PAN)$_2$] complex than for [Ni(PAN)Cl]. The three donor atoms of each ligand and the metal ion are in the same plane, as

Table 1
Selected distances, angles, and dihedral angles for complexes of PAN ligand with transitions metals M = Co(II), Ni(II), Cu(II), Zn(II); calculated in vacuum at B3LYP/6-31G(d,p) level.

Complex[a]	[Co(PAN)Cl]	[Ni(PAN)Cl]	[Cu(PAN)Cl][20]	[Zn(PAN)Cl]
Distance (Å)				
M—Cl	2.182	2.160	2.198	2.186
M—N(18)	1.836	1.828	1.969	2.056
M—N(27)	1.929	1.886	1.996	2.091
M—O	1.869	1.860	1.951	1.996
Angle (°)				
O—M—N(18)	85.34	85.64	82.05	85.34
N(18)—M—N(27)	81.51	82.45	78.89	75.90
N(27)—M—Cl	97.41	97.33	98.82	104.90
Cl—M—O	95.74	94.57	100.26	113.02
Dihedral angle (°)				
C(9)—N(18)—M—N(27)	179.95	180.00	179.55	163.33
C(22)—N(27)—M—N(18)	179.97	179.90	179.89	176.10
C(14)—O—M—Cl	179.99	179.99	177.91	127.81
C(9)—N(18)—N(19)—C(20)	179.98	180.00	179.73	168.93
C(22)—N(27)—M—Cl	0.08	0.02	1.31	34.25
N(27)—N(18)—O—M	0.07	0.00	0.83	24.46
O—N(18)—N(27)—Cl	0.30	0.00	1.77	45.93
C(9)—C(14)—O—M	0.05	0.01	0.73	16.31

[a] Atom numbering as referred in Fig. 1.

confirmed by the values of the dihedral angles: C(20)—N(19)—N(18)—Ni, C(39)—N(41)—N(42)—Ni, O(17)—N(18)—N(27)—Ni, and O(49)—N(42)—N(36)—Ni. The dihedral angles N(18)—N(19)—C(20)—C(27) and N(19)—N(18)—C(9)—C(14) show that in each ligand both aromatic moieties are co-planar. The deviations from the perfect octahedral geometry are demonstrated by the angles: O(17)—Ni—N(27) and N(36)—Ni—O(49).

The tetrahedral geometry for the nickel(II) complex was also tested as a starting point for energy minimization. In this case, PAN acts as a bidentate ligand [40] coordinating with the metal through the hydroxyl oxygen atom and one of the azo-group nitrogen atoms, creating six-membered ring. The pyridine nitrogen atom was outside the coordination sphere. This alternative geometry was found to be less stable than that presented here by about 26 kcal mol^{-1}.

The possible arrangement of the complexes in the zeolite channels and cavities was also an important aspect of the DFT calculations. In this context, the linear dimensions of the complex were calculated (as illustrated in Fig. 3). The values of the linear dimensions are as follows: for the PAN ligand x – 12.20 Å, y – 8.28 Å, z – 2.86 Å, for the [M(PAN)Cl] complexes (M = Co^{2+}, Ni^{2+}, Cu^{2+}) $x \sim 12.2$ Å, $y \sim 8.2$ Å, $z \sim 0.8$ Å, for octahedral nickel(II) complex x – 16.61 Å, y – 8.06 Å, z – 9.41 Å, and for the zinc(II) complex x – 12.03 Å, y – 7.96 Å, z – 2.70 Å. All [M(PAN)Cl] type complexes are bigger than the zeolite channels (~7.5 Å), but smaller than zeolite cavity (~13.0 Å). This prevents the complex from coming out of the material into the reaction medium (Fig. 4). In case of the [$Ni(PAN)_2$] complex, due to its dimensions, most probably only the chromophore is localized in the zeolite cavity and aromatic rings from PAN ligands occupy the zeolite channels, which makes this complex a bit less mobile than the others.

3.2. Characterization of the heterogeneous catalysts

Analysis of the SEM micrographs of the NaY and the guest–host catalysts indicates that there are no changes in the zeolite morphology or structure upon complex encapsulation [20–22]. SEM results also confirm that Soxhlet extraction is a suitable method for

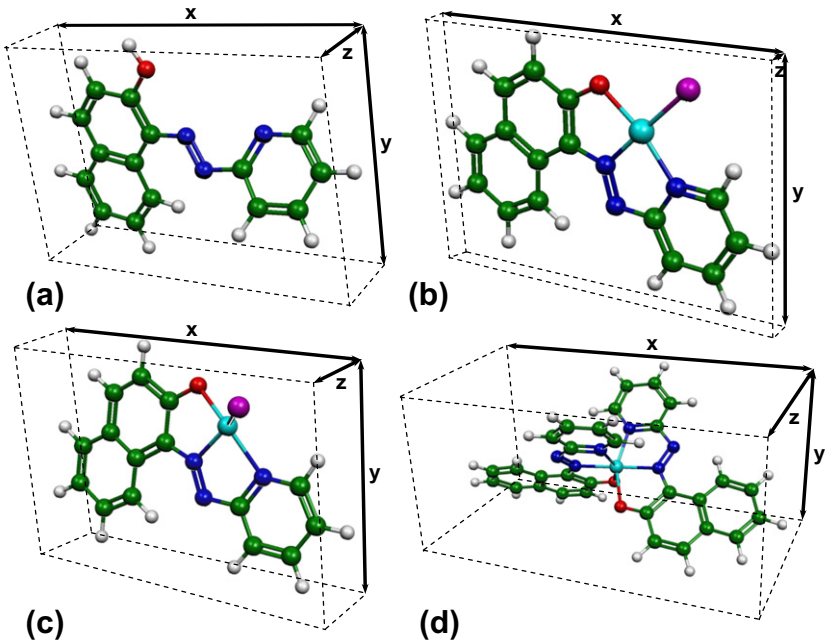

Fig. 3. Optimized structure of: (a) PAN ligand, (b) [M(PAN)Cl] complex (M = Co^{2+}, Ni^{2+}, Cu^{2+}), (c) [Zn(PAN)Cl] complex and (d) [$Ni(PAN)_2$] complex (B3LYP/6-31G(d,p) level of calculation). The shaded box indicates the molecular size and volume.

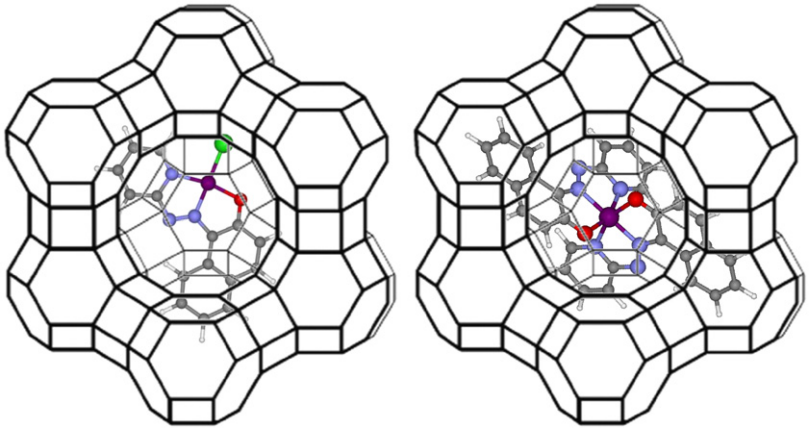

Fig. 4. Scheme of the encapsulated [$M(PAN)_n$] complexes in Y zeolite (see the abbreviations in Fig. 3 and Table 3).

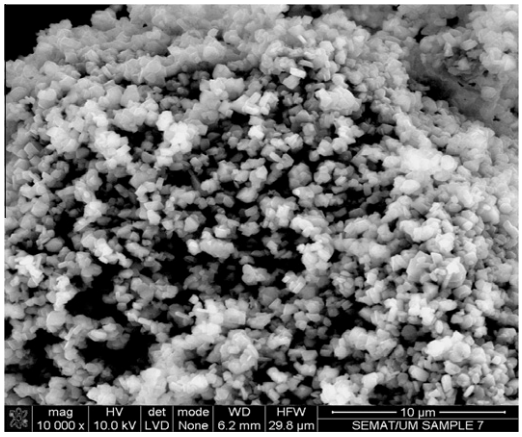

Fig. 5. SEM micrograph of [Ni(PAN)2]@Y (as an representative example).

removing the species adsorbed on the external surface of zeolite. It is clear from the micrographs that zeolite-entrapped metal complex has well-defined crystals and there is no indication of the presence of any metal ions, ligand, or complexes on the surface. Fig. 5 presents the field emission scanning electron micrographs of $[Ni(PAN)_2]$@Y as a representative example.

The FTIR patterns of all guest–host catalysts are very similar and are dominated by the strong bands assigned to the vibration of zeolite structure [20,22,41–43]. The broad band in 3700–3300 cm^{-1} is attributed to surface hydroxyl groups, while bands corresponding to the lattice vibrations are observed between 1300 and 450 cm^{-1}. No shift or broadening of the NaY vibrations associated with the structure was observed upon *in situ* synthesis of the Ni(II) and Zn(II) complexes, which provides evidence that the matrix remains unchanged upon encapsulation of the complexes, as observed for Cu(II) and Co(II) complexes [20,21]. Table 3 summarizes the positions of selected FTIR vibrations from neat and encapsulated complexes in the 1650–1150 cm^{-1} region where the zeolite matrix does not absorb. The intensities of peaks due to encapsulated complexes are weak because of their low concentrations in zeolite host [20,43].

The presence of these new bands suggests that in all cases the complexes are successfully encapsulated within the zeolite cages. The vibration frequency shifts could be caused by slight changes in the complex structure due to the zeolite cavity. The elemental analysis confirms that the metal:ligand ratio is 1:1 for neat and encapsulated Zn(II), Cu(II), and Co(II) complexes. Unexpectedly for the encapsulated Ni(II) complex, the metal:ligand ratio 1:2 was found. Nevertheless, the synthesis of the neat Ni(II) complex under the conditions applied for encapsulations leads to a complex with a 1:2 nickel:PAN molar ratio. Thus, the molecular structure of neat Ni(II) complex is retained in the zeolite host.

Table 4
Chemical analysis of $[M(PAN)_n]$@Y samples.

Material	Elemental analysis (wt.%)					Si/Al[b]
	M[a]	C[a]	N[a]	M/C		
[Co(PAN)]@Y [c]	1.40	1.43	0.29	0.97	(0.33)[d]	2.62
$[Ni(PAN)_2]$@Y	1.00	5.62	1.28	0.18	(0.32)[d] (0.16)[e]	2.62
[Cu(PAN)]@Y [f]	0.62	1.71	0.38	0.36	(0.35)[d]	2.79
[Zn(PAN)]@Y	1.60	0.55	0.12	2.90	(0.36)[d]	2.62

[a] Carbon, nitrogen, and metal obtained from bulk analysis (ICP-AES).
[b] Obtained from FTIR spectra of as-prepared materials using the formula: Si/Al = $(1/\chi) - 1$, where $\chi = 3.857 - 0.00621 \times \omega_{DR}$ [46,47].
[c] Values from Ref. [21].
[d] Value in parentheses refers to the theoretical ratio M/C (w/w) in the metal complex for a 1:1 stoichiometry.
[e] 1:2 stoichiometry.
[f] Values from Ref. [20].

Chemical analysis of [M(PAN)]@Y samples has confirmed the presence of metal in the zeolite framework. The same procedure resulted in different encapsulation efficiency, i.e., 26%, 46%, 64%, and 66% for Cu(II), Ni(II), Co(II), and Zn(II), respectively. As a consequence, the highest metal loading was obtained for [Zn(PAN)]@Y (Table 4).

However, fractions of uncomplexed Zn^{2+} and Co^{2+} [21] were also observed. The fact that these fractions could still be present at certain sites of the zeolite cannot ruled be out. Y zeolite has two sites inside the hexagonal prism and sodalite cages where cations can be accommodated and solvated by the zeolite oxygen atoms, but they cannot participate in the formation of the Zn(II) or Co(II) complexes due to steric constraints [44]. Only those Zn^{2+} and Co^{2+} located inside the supercages are available to interact with PAN, forming the complexes [21,44,45]. The migration of some metal ions from the supercages to the sodalite cages was observed for Fe(III) complexes of pyridazine derivatives assembled inside the zeolite Y [43].

All guest–host catalysts present similar Si/Al ratios obtained from the analysis of the FTIR data [46,47], Table 4. The Si/Al ratio in catalysts did not change substantially upon metal complexes encapsulation, indicating that dealumination does not occur during the *in situ* procedures.

3.3. Catalytic behavior of the guest–host catalysts

3.3.1. Oxidation of cyclohexene

Cyclohexene is prone to both epoxidation and allylic oxidation. The latter arises from a competition between the allylic C—H and the C=C double bonds of the alkene for the active oxidant, and consequently, the product distribution depends on the oxidant, solvent, and nature of catalyst [48]. To provide evidence for or against a radical mechanism and to evaluate the catalyst selectivity, oxygenation of cyclohexene was performed. The observed reaction products were identified as 2-cyclohexene-1-ol (CyOL),

Table 3
Selected infrared band positions and assignment for $[M(PAN)_n]$ (n = 1 or 2) complexes: calculated (DFT), neat, and as-prepared (encapsulated onto zeolite); calculated in vacuum using B3LYP at 6–31G(d,p) basis set[a].

Assignment	Cobalt(II) complex			Nickel(II) complex			Copper(II) complex			Zinc(II) complex		
	Calc.	Neat[b]	Encap[b]	Calc.	Neat	Encap.	Calc.	Neat[c]	Encap[c]	Calc.	Neat	Encap.
nCC	1505	1500	1508	1515	1520	1520	1520	1510	1514	1517	1508	1516
$\Delta(CH) + \nu(CC)$	1469	1469	1471	1483	1477	1479	1458	1445	1447	1458	1439	ND
$N(CC)_n + \nu(CN)_n + \nu(C_pN) + \nu(C_nN)$	1364	1365	1369	1359	1350	1350	1363	1358	1367	1372	1377	1384
$N(NN)_a + \nu(CC)_n + \nu(CO)$	1319	1311	1313	1319	1315	1317	1320	1324	1331	1322	1315	ND
$N(CC)_p + \nu(C_nN)$	1248	1256	~1250	1243	1254	1256	1246	1253	1256	1245	1252	ND

[a] ν—stretching mode; δ—bending mode; a—azo, p—pyridine; n—naphthol, Calc. = from DFT calculations, Encap. = complex encapsulated into zeolite matrix, ND – not detected.
[b] From Ref. [21].
[c] From Ref. [20].

2-cyclohexene-1-one (CyONE), and 1-*tert*-butylperoxy-2-cyclohexene (CyOX), which are the typical expected products for this reaction [49]. The results of experiments using new heterogeneous catalysts, denoted as [M(PAN)]@Y (where M = Co, Ni, Cu, Zn), in the oxidation of cyclohexene are shown in Table 5.

Cyclohexene is oxidized very slowly by tBuOOH under aerobic conditions, and the maximum conversion to allylic oxidation products, 2-cyclohexene-1-ol and 2-cyclohexene-1-one, is low. Another significant product in this reaction is 1-*tert*-butylperoxy-2-cyclohexene. NaY and the blank experiments were performed, and the same cyclohexene conversion was observed (14%). Only an allylic oxidation product has occurred with the formation of 1-*tert*-butylperoxy-2-cyclohexene. This product has been characterized before [48] and provides rather strong evidence for the involvement of $tBuOO^{\cdot}$ radical as a reactive intermediate. Marked improvements in substrate conversion when compared with [M(PAN)]@Y have resulted from the presence of metal PAN complexes. The heterogeneous catalysts increase the substrate conversion by a factor of 2.5, 1.9, 2.0, and 2.7 for the guest–host catalysts with cobalt, nickel, copper, and zinc complexes, respectively. Also, the formation of allylic oxidation products, 2-cyclohexene-1-ol and 2-cyclohexene-1-one, is much faster and the conversion to the ketone is higher (Table 5). The selectivity analysis shows that the 1-*tert*-butylperoxy-2-cyclohexene (CyOX) is an unstable product, while the 2-cyclohexene-1-one (CyONE) appears as a secondary and stable product [49]. It was found that [Cu(PAN)]@Y and [Zn(PAN)]@Y catalysts selectively oxidize cyclohexene to 2-cyclohexene-1-one, similar to other copper(II) heterogenized catalysts reported in [48]. Nevertheless, [Co(PAN)]@Y and $[Ni(PAN)_2]$@Y catalysts show higher ketone selectivity than [Cu(PAN)]@Y and [Zn(PAN)]@Y.

The oxidation of cyclohexene was also studied by Niasari and co-workers [14,33,50] with different complex-based heterogeneous catalysts using tBuOOH as radical initiator in variety of solvents. The authors found that regardless of the solvent used and the donor atoms set around the metal center, the conversion of cyclohexene changed according to the following metal order: Mn > Co > Cu > Ni. This series is in agreement with our study where the substrate conversion decreases in the order Zn > Co > Cu > Ni when the reactions proceed in the heterogeneous phase. The low catalytic activity (TON) of the nickel(II) complex can be explained by the DFT calculations (see the previous section). Accordingly, nickel(II) formed six-coordinated pseudo-octahedral complex in the zeolite cavity with the aromatic rings from the ligand moiety occupying the zeolite channels (Figs. 3 and 4). This makes the diffusion of reactants to the active site more difficult than when the complexes have a planar structure and they are localized mainly in the zeolite cavity.

The radical mechanism of this catalytic reaction involves the formation of intermediates by the coordination of oxygen atom from the oxidant. The lack of accessible coordination sites in the pseudo-octahedral nickel(II) complex makes it rather inactive. Nevertheless, based on DFT data, the formation of a four-coordinated complex cannot be excluded, especially inside the zeolite matrix that can stabilize this geometry, although in lower concentrations. Thus, the observed catalytic performance of the encapsulated nickel(II) PAN complex could be attributed to the presence of the four-coordinating species with the available coordination sites.

The high substrate conversion in the presence of the [Zn(PAN)]@Y catalyst containing a redox-inactive central zinc(II) ion might be attributed to enzymatic behavior of complex. The product formation might be due to formation of an active species ($Zn^{(II)}$-PAN-PhOO$^{\cdot}$) by the interaction of tBuOOH with the oxygen donor (from ligand) and further coordination to the metal. The subsequent interactions of active species with cyclohexene produced intermediates ($Zn^{(II)}$-PAN-Cy-PhOO$^{\cdot}$) [51,52].

When reaction was running in the homogeneous phase, the zinc catalyst shows the lowest cyclohexene conversion. This might be due to partial decomposition of the ligand and/or formation of inactive species in the reaction media.

In the heterogeneous phase, the accessibility to the active sites is difficult due to diffusion constraints imposed on substrates and reactants by the porous network of the host. On other hand, the use of heterogeneous solid catalysts did not damage the solid during the course of the reaction and finally lead to a higher substrate conversion and TON than in the homogeneous phase. The oxidation products found by the authors of references [14,33,50] were the same as found in this work; no cyclohexene epoxide was detected in all experiments mentioned when tBuOOH was used as oxidant. The authors state that when hydrogen peroxide was used as radical initiator, the epoxide was formed in high yield, due to the strength of O—O bond in H_2O_2 [13]. Lack of epoxide formation opposes the statement that in apolar solvents the epoxide is formed as a primary product and other products are formed as a consequence of sequential oxidation. Nevertheless, when a gold base catalyst in toluene was applied for the oxidation of cyclohexene, again only the allylic oxidation products were formed [53]. The authors show that the toluene is not involved intimately with the reaction and that the solvent does not act as sacrificial source of hydrogen in the rate-determining step, in contrast to that of propene oxidation. This apparently took place in our study because we successfully use toluene as an internal standard.

Table 5
Conversion of cyclohexene and selectivity of the various oxidation products after 48 h of reaction time.

Catalyst	Conversion (%)	Selectivity (%)			TON[f]
		CyOL[c]	CyONE[d]	CyOX[e]	
–	14	–	–	100	–
NaY	14[a]	–	–	100	–
[Co(PAN)]@Y	35	2	21	77	34.5
$[Ni(PAN)_2]$@Y	26[b]	9	19	73	27.8
[Cu(PAN)]@Y	28	–	11	89	56.7
[Zn(PAN)]@Y	38	–	5	95	38.6
[Co(PAN)Cl]	59	–	35	65	97.8
$[Ni(PAN)_2]$	15	18	12	70	34.7
[Cu(PAN)Cl]	26	–	32	68	83.4
[Zn(PAN)Cl]	13[a]	6	8	86	21.1

[a] Reaction time 24 h.
[b] Reaction time 70 h.
[c] CyOL is 2-cyclohexene-1-ol product.
[d] CyONE is 2-cyclohexene-1-one product.
[e] CyOX is 1-*tert*-butylperoxy-2-cyclohexene product.
[f] TON = the converted cyclohexene (mol)/the amount of metal ions in the added catalyst (mol) with allowance for the background reaction.

3.3.2. Oxidation of cyclohexanol

The oxidation of cyclohexanol is negligible in the absence of heterogeneous transition metal catalysts, confirming that under the conditions of the experiments, the oxidation is indeed catalytic in nature. The zeolite NaY without encapsulated metal complexes is also catalytically inactive. Thus, the determining role is played by metal PAN complexes encapsulated into the zeolite. The results in Table 6 show an enhancement of the conversion percentages

Table 6
Oxidation of cyclohexanol to cyclohexanone with tBuOOH by the guest–host catalysts.

Catalyst	Time (h)	Conversion (%)	Yield (%)	TON
[Co(PAN)]@Y	4	32	32	76.8
$[Ni(PAN)_2]$@Y	3	39	39	135.5
[Cu(PAN)]@Y	3	46	46	272.2
[Zn(PAN)]@Y	5	51	51	119.9

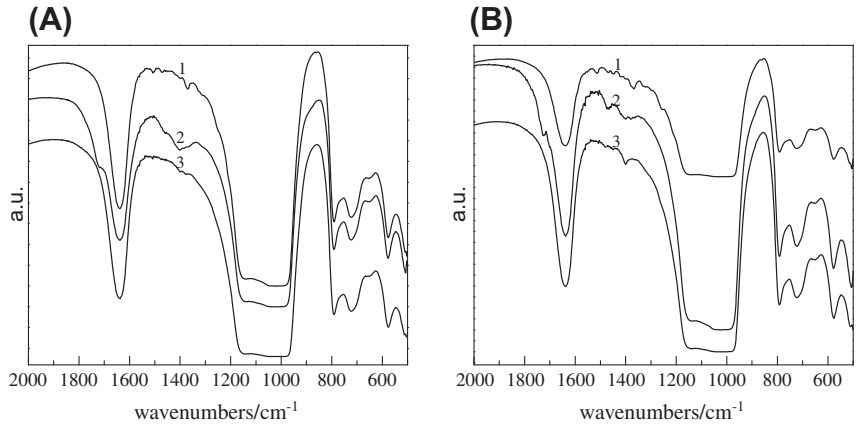

Fig. 6. Comparison of FTIR spectra in 2000–500 cm^{-1} region, 1-before catalytic test, 2-after cyclohexene oxidation, 3-after cyclohexanol oxidation: (A) [Co(PAN)]@Y; (B) [Cu(PAN)]@Y.

from 32% to more than 51% in the presence of [Co(PAN)]@Y and [Zn(PAN)]@Y, respectively. In cyclohexanol oxidation was observed one reaction product, cyclohexanone.

It is known that transition metal complexes and their loading (when they are heterogenized) and also the supporting materials have a big influence on the catalytic activity in the oxidation of organic molecules including cyclohexanol [54–56]. The trend observed in the substrate conversion and product yield follows the empirical Irving–Williams order [57] $Co^{2+} < Cu^{2+} > Zn^{2+}$. This might be due to the fact that the transition state of the oxidation of cyclohexanol reaction resembles the structure of a metal–PAN complex [58]. The coordination mode of nickel(II) PAN complex is different from others metals studied in a zeolite host. Based on the DFT calculations, it has mainly a pseudo-octahedral geometry, whereas others are four-coordinated planar or slightly distorted planar. Because of this, we have to exclude the nickel(II) complex from the following comparison.

The heterogeneous catalysts used in the oxidation of cyclohexene and cyclohexanol were studied after the reaction run. All guest–host catalysts show the same behavior. As an example, the comparison of the FTIR spectra of [Co(PAN)]@Y and [Cu(PAN)]@Y catalysts before and after utilization cycle is presented in Fig. 6.

After catalytic oxidation of cyclohexene and cyclohexanol by [Co(PAN)]@Y and [Cu(PAN)]@Y, some band broadening is observed in range where the vibration bands for the complex occur (Fig. 6). Some decrease in the intensity of the bands due to the complex after catalytic run is clearly observed in [Zn(PAN)]@Y and $[Ni(PAN)_2]$@Y. This suggests that some complexes leach into the reaction medium and/or the degradation of the complexes under catalytic reaction conditions occurs. Chemical analysis, after the catalytic run, of [Cu(PAN)]@Y, $[Ni(PAN)_2]$@Y, [Co(PAN)]@Y, and [Zn(PAN)]@Y catalysts suggests a leaching of the complex after the oxidation of cyclohexene at 3, 28, 97, and 99%, respectively. No leaching was observed for the copper complex after oxidation of cyclohexanol. Other complexes leached into reaction media: [Co(PAN)]@Y (14.3%), [Zn(PAN)]@Y (18.8%) and $[Ni(PAN)_2]$@Y (63.0%). The oxidant used can have some destructive effect on the guest–host catalysts. Although the situation is not entirely clear, some major effects can be pointed out. The harmful effect of tBuOOH on the heterogeneous catalysts seems to act at the level of active-phase leaching but does not lead to zeolite structure damage. Nevertheless under both oxidation reaction conditions, the [Cu(PAN)]@Y catalyst is most stable in term of complex leaching. For all heterogeneous catalysts studied, the infrared spectra in the range typical for the zeolite host do not show significant changes after the catalytic reaction. This suggests that no structural changes on the zeolite host took place during the catalytic reaction.

4. Conclusions

Transition metal complexes with PAN ligand have been encapsulated in NaY zeolite by the *flexible ligand* method. The complexes are mainly physically entrapped throughout the framework and slightly distorted due to physical constrains imposed by the structure and/or owing to host–guest interactions. Encapsulation of metal complexes in NaY has a marked effect on the activity of cobalt(II), nickel(II), copper(II), and zinc(II) complexes in the oxidation of cyclohexene and cyclohexanol to the corresponding products. The catalytic results prove that these guest–host catalysts have activity for the oxidation reactions using tBuOOH as an oxidant. In general, the metal complexes encapsulated are more active in cyclohexanol oxidation where the catalytic activities are in agreement with the Irving–Williams series. It was proven experimentally that the heterogenized Zn(II) complex is the best catalyst among the four complexes analyzed; in addition, it was shown that it possesses distinct geometrical features. For both oxidations, [Zn(PAN)]@Y catalyst shows the highest substrate conversion, contrary to the homogeneous phase where the conversion is very low, most probably due to partial ligand decomposition. The low catalytic activity of nickel(II) in cyclohexene oxidation can be due to its localization into zeolite host. The balance between the heterogeneous and homogeneous character can explain the success of our catalysts.

Acknowledgments

This work was supported by the Centro de Química (University of Minho, Portugal) and by Fundação para a Ciência e Tecnologia (FCT-Portugal), under Programme POCTI-SFA-3-686. IKB thanks FCT for the contract under the Program Ciência 2007.

References

[1] C.E. Song, S. Lee, Chem. Rev. 102 (2002) 3495.
[2] A. Corma, H. Garcia, Eur. J. Inorg. Chem. 6 (2004) 1143.
[3] I.W.C.E. Arends, R.A. Sheldon, Appl. Catal. A 212 (2001) 175.
[4] D.E. Vos, M. Dams, B.F. Sels, P.A. Jacobs, Chem. Rev. 102 (2002) 3615.
[5] Q.-H. Xia, H.-Q. Ge, C.-P. Ye, Z.-M. Liu, K.-X. Su, Chem. Rev. 105 (2002) 1603.
[6] F. Bedioui, Coord. Chem. Rev. 144 (1995) 39.
[7] M. Salavati-Niasari, M. Shakouri-Arani, F. Davar, Micropor. Mesopor. Mater 116 (2008) 77.
[8] G. Li, L. Chen, J. Bao, T. Li, F. Mei, Appl. Catal. A 346 (2008) 134.
[9] P.K. Saha, S. Koner, Inorg. Chem. Commun. 7 (2004) 1164.

[10] B. Fan, H. Li, W. Fan, C. Jin, R. Li, Appl. Catal. A 340 (2008) 67.
[11] M.R. Maurya, A.K. Chandrakar, S. Chand, J. Mol. Catal. A: Chem. 270 (2007) 225.
[12] M.R. Maurya, M. Kumar, A. Kumar, J. Costa Pessoa, Dalton Trans. (2008) 4220.
[13] M. Salavati-Niasari, F. Farzaneh, M. Ghandi, J. Mol. Catal. A: Chem. 186 (2002) 101.
[14] M. Salavati-Niasari, M. Shaterian, M. Reza Ganjali, P. Norouzi, J. Mol. Catal. A: Chem. 261 (2007) 147.
[15] R. Ganesan, B. Viswanathan, J. Mol. Catal. A: Chem. 223 (2004) 21.
[16] V. Mahdavi, M. Mardani, M. Malekhosseini, Catal. Commun. 9 (2008) 2201.
[17] M.L. Parentis, N.A. Bonini, E.E. Gonzo, React. Kinet. Catal. Lett. 76 (2002) 243.
[18] G. Bai, C. Jia, K. Xu, X. Fan, H. Ning, K. Zhao, React. Kinet. Catal. Lett. 96 (2009) 109.
[19] H. Adams, R.M. Bucknall, D.E. Fenton, M. Garcia, J. Oakes, Polyhedron 17 (1998) 4169.
[20] P. Parpot, C. Teixeira, A.M. Almeida, C. Ribeiro, I.C. Neves, A.M. Fonseca, Micropor. Mesopor. Mater 117 (2009) 297.
[21] C. Teixeira, P. Parpot, I.C. Neves, A.M. Fonseca, Mater. Sci. Forum 109 (2008) 587.
[22] N. Nunes, R. Amaro, F. Costa, E. Rombi, M.A. Carvalho, I.C. Neves, A.M. Fonseca, Eur. J. Inorg. Chem. 12 (2007) 1682.
[23] A.D. Becke, J. Chem. Phys. 98 (1993) 5648.
[24] A.D. Becke, Phys. Rev. A 38 (1988) 3098.
[25] C. Lee, W. Yang, R.G. Parr, Phys. Rev. B 37 (1988) 785.
[26] P.J. Stevens, F.J. Devlin, C.F. Chabalowski, M.J. Frisch, J. Chem. Phys. 98 (1994) 11623.
[27] W.F. Murphy, F. Zerbetto, J.L. Duncan, D.C. McKean, J. Phys. Chem. 97 (1993) 581.
[28] G. Rauhut, P. Pulay, J. Phys. Chem. 99 (1995) 3093.
[29] J.P. Merrick, D. Moran, L. Radom, J. Phys. Chem. A 111 (2007) 11683.
[30] Gaussian03, Revision C.02, M.J. Frisch, G.W. Trucks, H.B. Schlegel, G.E. Scuseria, M.A. Robb, J.R. Cheeseman, J.A. Montgomery, Jr., T. Vreven, K.N. Kudin, J.C. Burant, J.M. Millam, S.S. Iyengar, J. Tomasi, V. Barone, B. Mennucci, M. Cossi, G. Scalmani, N. Rega, G.A. Petersson, Nakatsuji, H., M. Hada, M. Ehara, K. Toyota; R. Fukuda; J. Hasegawa, M. Ishida, T. Nakajima, Y. Honda, O. Kitao, H. Nakai, M. Klene, X. Li, J.E. Knox, H.P. Hratchian, J.B. Cross, V. Bakken, C. Adamo, J. Jaramillo, R. Gomperts, R.E. Stratmann, O. Yazyev, A.J. Austin, R. Cammi, C. Pomelli, J.W. Ochterski, P.Y. Ayala, K. Morokuma, G.A. Voth, P. Salvador, J.J. Dannenberg, V.G. Zakrzewski, S. Dapprich, A.D. Daniels, M.C. Strain, O. Farkas, D.K. Malick, A.D. Rabuck, K. Raghavachari, J.B. Foresman, J.V. Ortiz, Q. Cui, A.G. Baboul, S. Clifford, J. Cioslowski, B.B. Stefanov, G. Liu, A. Liashenko, P. Piskorz, I. Komaromi, R.L. Martin, D.J. Fox, T. Keith, M.A. Al-Laham, C.Y. Peng, A. Nanayakkara, M. Challacombe, P.M.W. Gill, B. Johnson, W. Chen, M.W. Wong, C. Gonzalez, J.A. Pople, Gaussian, Inc., Wallingford CT, 2004.
[31] P. Flükiger, H.P. Lüthi, S. Portmann, J. Weber, MOLEKEL 4.3: Molecular Visualization Software, Swiss Center for Scientific Computing, Manno, Switzerland, 2000.
[32] Computer Program Gauss View Ver.03, Gaussian Inc., Pittsburg, PA 15106, USA.
[33] M. Salavati-Niasari, H. Babazadeh-Arani, J. Mol. Catal. A: Chem. 274 (2007) 58.
[34] M. Salavati-Niasari, Trans. Met. Chem. 33 (2008) 443.
[35] S. Basu, S. Halder, I. Pal, S. Samanta, P. Karmakar, M.G.B. Drew, S. Bhattacharya, Polyhedron 27 (2008) 2943.
[36] R.D. Shannon, Acta Crystallogr., Sect. A 32 (1976) 751.
[37] A.S. Burlov, A.S. Antsyshkina, G.G. Sadikov, L.N. Divaeva, A.D. Garnovskii, V.S. Sergienko, Russ. J. Coord. Chem. 26 (2000) 648.
[38] L.C. Emeleus, D.C. Cupertino, S.G. Harris, S. Owens, S. Parsons, R.M. Swart, P.A. Tasker, D.J. White, J. Chem. Soc. Dalton Trans. (2001) 1239.
[39] N.W. Alcock, R.C. Spencer, R.H. Prince, O. Kennard, J. Chem. Soc. A (1968) 2383.
[40] G. Supriyanto, J. Simon, Talanta 68 (2005) 318.
[41] H. Figueiredo, M.M.M. Raposo, A.M. Fonseca, I.C. Neves, C. Quintelas, T. Tavares, Stud. Surf. Sci. Catal. 158 (2005) 1073.
[42] H. Figueiredo, I.C. Neves, C. Quintelas, T. Tavares, M. Taralunga, J. Mijoin, P. Magnoux, Appl. Catal. B: Environ. 66 (2006) 274.
[43] H. Figueiredo, B. Silva, M.M.M. Raposo, A.C. Fonseca, I.C. Neves, C. Quintelas, T. Tavares, Micropor. Mesopor. Mater 109 (2008) 163.
[44] M. Alvaro, B. Ferrer, H. Garcia, A. Sanjuan, Tetrahedron 55 (1999) 11895.
[45] N. Xiao, Q. Xu, J. Sun, J. Chen, J. Chem. Soc. Dalton Trans. (2006) 603.
[46] W. Lutz, C.H. Ruscher, D. Heidemann, Micropor. Mesopor. Mater. 55 (2002) 193.
[47] G.C. Ghesti, J.L. Macedo, V.C.I. Parente, J.A. Dias, S.C.L. Dias, Micropor. Mesopor. Mater. 100 (2007) 27.
[48] G. Olason, D.C. Sherrington, React. Funct. Polym. 42 (1999) 163.
[49] H. Figueiredo, B. Silva, C. Quintelas, M.M.M. Raposo, P. Parpot, A.M. Fonseca, A.E. Lewandowska, M.A. Bañares, I.C. Neves, T. Tavares, Appl. Catal. B: Environ. 94 (2010) 1.
[50] M. Salavati-Niasari, M. Shaterian, J. Porous. Mater. 15 (2008) 581.
[51] P. Chaudhuri, M. Hess, J. Mu1ller, K. Hildenbrand, E. Bill, T. Weyhermu1ller, K. Wieghardt, J. Am. Chem. Soc. 121 (1999) 9599.
[52] K.C. Gupta, A. Kumar Sutar, C.-C. Lin, Coord. Chem. Rev. 253 (2009) 1926.
[53] M.D. Hughes, Y.-J. Xu, P. Jenkins, P. McMorn, P. Landon, D.I. Enache, A.F. Carley, G.A. Attard, G.J. Hutchings, F. King, E.H. Stitt, P. Johnston, K. Griffin, Ch.J. Kiely, Nature 437 (2005) 1132.
[54] M. Salavati-Niasari, E. Zamani, M.R. Ganjali, P. Norouzi, J. Mol. Catal. A: Chem. 261 (2007) 196.
[55] C.N. Kato, M. Hasegawa, T. Sato, A. Yoshizawa, T. Inoue, W. Mori, J. Catal. 230 (2005) 226.
[56] T. Iwahama, Y. Yoshino, T. Keitoku, S. Sakaguchi, Y. Ishii, J. Org. Chem. 65 (2000) 6502.
[57] H. Irving, R.J.P. Williams, J. Chem. Soc. (1953) 3192.
[58] R.K.O. Sigel, A.M. Pyle, Chem. Rev. 107 (2007) 97.